






# Deep-water corals indicate the Red Sea survived the last glacial lowstand

Morgan I. Chakraborty<sup>a,1</sup>, Arash Sharifi<sup>a,b</sup>, Francesca Benzonì<sup>c</sup>, François L. H. Tissot<sup>d</sup> , Ali Pourmand<sup>a</sup>, Marco Taviani<sup>e,f</sup> , Bolton Howes<sup>g</sup> , Peter K. Swart<sup>a</sup>, Chaojin Lu<sup>a</sup>, Mattie Rodrigue<sup>g</sup>, and Sam J. Purkis<sup>a</sup>

Affiliations are included on p. 8.

Edited by James Kennett, University of California Santa Barbara, Santa Barbara, CA; received August 1, 2024; accepted January 9, 2025

The Red Sea, a nascent ocean basin connected to the Indian Ocean via a shallow strait, is assumed to have experienced significant environmental changes during the last glacial period due to a sea-level drop likely exceeding 110 m. This study investigates the hypothesis that hydrodynamic restriction led to severe ecological impacts, including basin-wide extinction due to elevated salinity followed by a short time of oxygen depletion. Uranium–Thorium dating of deep-water corals (DWCs) from 26 northern Red Sea sites reveals coral growth during and after the Last Glacial sea-level lowstand, indicating tolerable seawater chemistry. Additional geochemical data show no significant difference in Red Sea chemistry or temperature between the Latest Pleistocene and Holocene. A meta-analysis of 27 deep-sea cores reveals that while planktonic foraminifera experienced local extinction, other microfossil groups seemingly persisted. These findings suggest that the Red Sea survived the last sea-level lowstand, challenging the paradigm of a complete ecological collapse and providing insights into the resilience of marine ecosystems.

Red Sea | last glacial maximum | deep-sea corals | geochemistry

The Red Sea connects to the Indian Ocean via the 20-km-wide Strait of Bab-el-Mandeb. The shallowest part of this connection, the Hanish Sill, is only 137 m deep. Evaporation exceeds the freshwater input, and marine conditions are only safeguarded by seawater inflowing from the Indian Ocean, making the Red Sea Earth's warmest and saltiest "normal" marine basin. Lower glacioeustatic sea level is expected to reduce the strait's profile, thereby decreasing water–mass exchange with the Indian Ocean. A significant hindrance in this exchange would profoundly affect Red Sea temperature, chemistry, and ecology.

Seabed core studies indicate a significant increase in Red Sea salinity during the Pleistocene sea-level lowstands (1–7). The pelagic record (foraminifera, pteropods, and coccolithophorids) suggests salinity rose at least as high as 50 PSU (5–10) during the Last Glacial Maximum (LGM), defined by Clark et al. (11) to span 19.0 to 26.5 ky BP. The Red Sea "aplanktonic" interval (8, 12) is believed to be an ecological response to lethally high-salinity. Glacial-age sediments host dolomite and inorganically precipitated aragonite, possibly deposited during supersaturated conditions (13, 14), and evidence from fossil reefs indicates important faunal changes between the last interglacial and Holocene biota (15). In the last 13 ky, faunal [pteropods (16)] and sedimentological [sapropel (3, 6, 10, 17)] evidence document episodes of bottom-water stagnation and oxygen depletion. Obviously, these oceanographic scenarios strongly reverberated upon the basin's biota. At the extreme, Klausewitz (18) suggests the Red Sea resembled a hypersaline lake during the last (and presumably penultimate) glacial sea-level lowstands.

All together, these arguments have been taken as indication of basin-wide extinction of shallow-water fauna (15, 19), logically extending to extinction in deep water too (20). Under this scenario, Holocene recolonization of the Red Sea fauna would only have started ~15 ky BP, with the re-establishment of normal marine conditions facilitated by rising sea level and unfettered connection to the Indian Ocean. Yet, water stagnation and prolonged oxygen depletion at depth is known to exert strong control on deep sea benthos, like corals (21), up to local extinction (22).

For reasons still debated, planktonic forams possibly persisted through the last glacial lowstand in at least two refugia—the northern Gulf of Aqaba and the southern Red Sea (1, 12). Survival of these protists advocates that lowstand restriction did not completely sterilize the basin. Lowstand refugia are also supported by the exceptionally high levels of endemism for Red Sea fish and invertebrates (23–25). The coral central to this study, *Rhizosmilia valida*, is one such Red Sea endemic. Considering estimates of evolutionary rates, it is hard to reconcile that the abundance of endemics evolved only within the last

## Significance

The prevailing hypothesis suggests that life was extinguished in the Red Sea when sea level fell at least 110-m below present at the end of the Last Glacial period. This sterilization is thought to have occurred because that drop restricted the basin from the Indian Ocean, inducing a hyper-salinity crisis. Dating and geochemical analyses of deep-water corals which we collected during submersible dives, however, shows this delicate ecosystem to have thrived, even during the last sea-level minimum, with seawater temperature and chemistry broadly similar to today. Our findings challenge the paradigm of a complete ecological collapse in the Red Sea during the last sea-level lowstand. Our results imply that the basin's fauna endured for a longer timescale than earlier estimates.

Author contributions: M.I.C. and S.J.P. designed research; M.I.C., A.S., A.P., P.K.S., C.L., and S.J.P. performed research; M.I.C., F.B., M.T., B.H., M.R., and S.J.P. contributed new reagents/analytic tools; M.I.C., A.S., F.L.H.T., A.P., P.K.S., C.L., and S.J.P. analyzed data; and M.I.C. and S.J.P. wrote the paper.

The authors declare no competing interest.

This article is a PNAS Direct Submission.

Copyright © 2025 the Author(s). Published by PNAS. This article is distributed under [Creative Commons Attribution-NonCommercial-NoDerivatives License 4.0 \(CC BY-NC-ND\)](https://creativecommons.org/licenses/by-nc-nd/4.0/).

Although PNAS asks authors to adhere to United Nations naming conventions for maps (<https://www.un.org/geospatial/mapsgeo>), our policy is to publish maps as provided by the authors.

<sup>1</sup>To whom correspondence may be addressed. Email: [morgan.chakraborty@earth.miami.edu](mailto:morgan.chakraborty@earth.miami.edu).

This article contains supporting information online at <https://www.pnas.org/lookup/suppl/doi:10.1073/pnas.2415559122/-/DCSupplemental>.

Published February 18, 2025.

15 ky—unless they nimbly migrated back-and-forth between the Gulf of Aden and Red Sea as sea level oscillated.

A pair of hypotheses have been proposed to explain the creation of lowstand refugia. The first hypothesis states that intensified rainfall at the close of the last glacial tempered the high salinity induced by restriction (26–31). However, it is an open question as to whether wet periods follow glacial maxima or occur within them (32–34).

The second refugia hypothesis contends that the late glacial Bab-el-Mandeb was not completely closed (35), even when the sea level dropped >110 m below present between 18 and 20 ky BP (36–38). Bailey et al. (35) advocate connection to the Indian Ocean was maintained via a channel at least 4 km wide and 15 m deep. On this, Lambeck et al. (39) argue that the residual flow through this narrow channel would have been insufficient to prevent a major increase in Red Sea salinity and decrease in temperature during glacial maxima. Biton et al. (5), meanwhile, propose a more moderate sea-level drop of 105 m.

The primary evidence for glacial lowstand sterilization of the Red Sea, as well as possible refuges from it, comes from planktonic forams, and to some extent, pteropods. While useful, these data have at least three limitations. First, there are few seabed cores in the Red Sea from which forams have been counted compared to the large size of the basin. It would therefore seem premature to make conclusions about lowstand extinctions versus refugia. Second, the tolerance of forams to high salinity might not be representative of all normal marine biota. Appraising the persistence, or not, of other biota through the last sea-level lowstand would be informative. Third, planktonic forams only audit habitability of the shallow photic zone. Quantifying the glacial persistence of biota in deeper water would be illuminating.

To advance our understanding of glacial restriction on the Red Sea ecosystem, we have sampled deep-water coral (DWC) skeletons at 26 sites in the northern Red Sea (Fig. 1), an area considered to be outside of any possible refuge. Using Uranium–Thorium (U–Th) dating, we evaluated whether these deep-water, sessile, Scleractinia survived the last glacial lowstand. We further used clumped isotope thermometry, stable isotopes, and measurements of radiogenic strontium to determine the changing character of the seawater in which these DWCs lived. This unique dataset brings constraints on whether the ecological development of semi-restricted rift basins is interrupted by high-frequency sea-level oscillation. In particular, it allows us to arbitrate whether the exceptionally diverse (and endemic) modern Red Sea fauna has developed within the last ~15 ky, after the main deglaciation phase

reestablished connection to the Indian Ocean. Additionally, our findings shed light on the response of marine ecosystems during episodes of rapid environmental change.

## Results

**The Microfossil Evidence for LGM Red Sea Sterilization Is Equivocal.** Meta-analysis (Fig. 2) reveals that barren intervals of microfossils exist but vary among planktonic and benthic forams, pteropods, and coccolithophores (coccoliths). For planktonic forams, we do not find any barren intervals in any of the cores from the Gulf of Aqaba during sea-level lowstands. In contrast, such intervals appear in almost all north and central Red Sea cores during the LGM (Marine Isotope Stage—MIS 2) but only in three out of seven of those from the Penultimate Glacial Period (MIS 6). Five cores from the southern Red Sea lack planktonic intervals altogether. Planktonic forams were only absent in one core which penetrated MIS 4. During that marine isotope stage, eustatic sea level only fell to 100 m below present (40, 41) (Fig. 2A). Assuming the Hanish Sill to have situated at 137 m, as it does today, the MIS 4 lowstand should not have isolated the Red Sea and therefore would not be expected to be accompanied by faunal loss. Benthic forams persist through all the glacial lowstands. As do coccoliths, save for the northernmost core collected in the Gulf of Aqaba, in which they are reported briefly absent by Winter et al. (42) after the LGM, else shifted to species tolerant of high salinity (43, 44). Pteropods are only reported absent in two cores collected in the central Red Sea, both during the LGM.

**Uranium–Thorium Geochronology of Coral Skeletons.** During our submersible dives, we encountered the same abundant *R. valida* death assemblages (Fig. 3) as Qurban et al. (51). Rare live specimens occurred only as isolated colonies. Clearly, *R. valida* was much more abundant in the past than in the present. Based on our own observations, and specimens collected by Scheer and Pillai (52), this endemic DWC species occupies a depth range of 300 to 750 m, situating it within Red Sea Intermediate Waters, as defined by Sofianos and Johns (53). The lifespan of *R. valida* has yet to be determined, but we presume it to be measured on the scale of centuries as opposed to decades, as is common for deep-water Scleractinia (54). U–Th dates of our 26 coral samples are presented in Fig. 4 and **Dataset S1**. For samples older than 10 ky BP, the average 95% CI extend 488 years either side of the mean value. For the younger corals, the deviation is 137 years. We judge these uncertainties to be within acceptable limits to distinguish Pleistocene- vs. Holocene-aged corals.

Deep-water *R. valida* corals range in age from 0.8 to 17.8 ky BP, while *Leptoseris* corals exhibit a narrower age range of 0.9 to 7.8 ky BP. When these ages are compared against three sea-level records (36–38), seven *R. valida* corals are found to date back to the last Pleistocene lowstand. Notably, two of these samples predate the onset of rapid sea-level rise associated with the initiation of the main deglaciation phase around 16.5 ky BP (36) (Fig. 4A), with a further acceleration occurring after meltwater pulse 1a at 14.5 ky BP (55). DWCs clearly inhabited the N. Red Sea when connection to the Indian Ocean was restricted.

**Clumped Isotope Thermometry of Coral Skeletons.** Clumped isotope ( $\Delta_{47}$ ) thermometry examines the thermodynamically controlled “clumping” of  $^{13}\text{C}$  and  $^{18}\text{O}$  isotopes within the carbonate lattice (56, 57). Unlike conventional oxygen isotope paleothermometry,  $\Delta_{47}$  does not require knowledge of the  $\delta^{18}\text{O}$  values of the water in which the carbonate formed. Temperatures

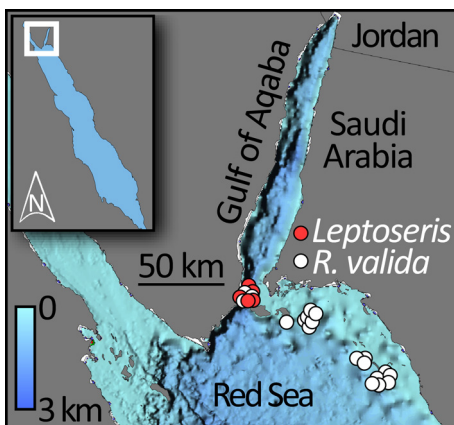


**Fig. 1.** Locations of sampled corals and seawater in the northern Red Sea. Two coral species were collected: *Rhizosmilia valida* from 20 sites at depths of 400 to 720 m, and *Leptoseris cf. striatus* from six sites at depths of 80 to 90 m.

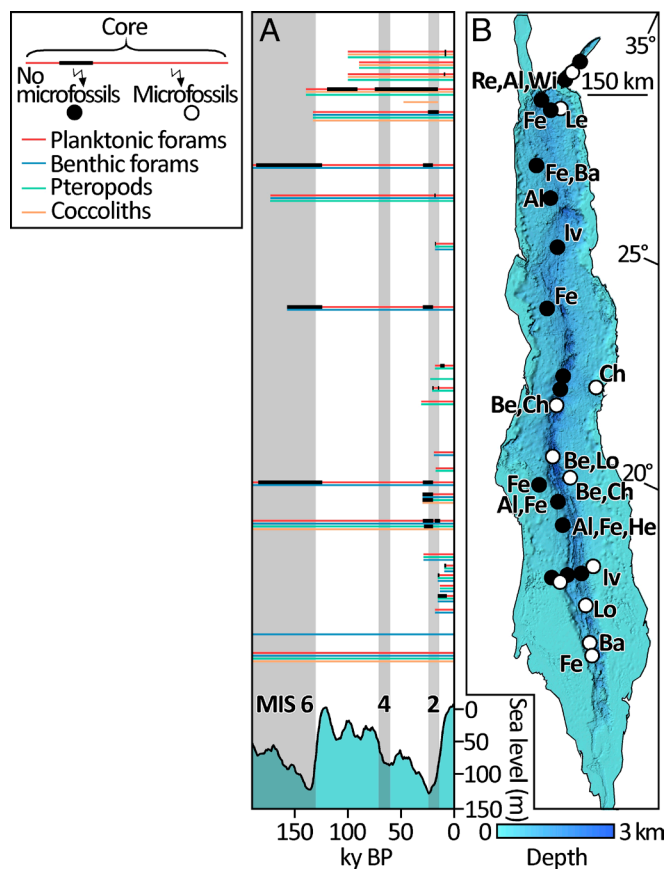


**Fig. 2.** Meta-analysis of Red Sea coring studies on the presence/absence of four microfossil groups: Planktonic and benthic foraminifera (forams), pteropods, and coccolithophores (coccoliths). (A) Horizontal colored lines indicate the persistence of each microfossil down-core, with black boxes marking intervals where microfossils are absent. Compiled as [Dataset S1](#). Gray bars represent sea-level lowstands. Sea-level curve from Rohling et al. (45). (B) Core locations in the Red Sea, as reported by Re = Reiss et al. (8), Fe = Fenton et al. (12), Ba = Badawi et al. (46), Le = Legge et al. (44), Wi = Winter et al. (42), He = Hemleben et al. (7), Lo = Locke and Thunel (1), Iv = Ivanova et al. (10), Al = Almogi-Labin et al. (9, 16, 47, 48), Be = Berggren and Boersma (49), Ch = Chen (50). Black circles indicate cores with intervals barren of microfossils; white circles indicate cores without barren intervals.

retrieved from our corals span 12.34 to 38.75 °C, with an average of 23.85 °C (Fig. 4B). This is somewhat warmer than the 21.35 °C modern average N. Red Sea temperature at 400 m depth measured during our 2020, 2022, 2023 summer/winter research cruises (31). Note,  $\Delta_{47}$  thermometry is accepted to have an external precision of  $\sim 0.01\text{‰}$ , equivalent to  $\sim 3$  °C (58). Corals exhibit species-specific isotope ordering in their aragonite, known as “vital effects,” unfortunately unknown for the species we sampled. A substantial deviation of the  $\Delta_{47}$  derived temperatures recorded by the corals is therefore eminently plausible.

To avoid overreaching our results, we rather consider the trend in temperature that the corals chart through time, as opposed to the absolute  $\Delta_{47}$  data. A linear fit through the data suggests the Red Sea to have warmed by  $\sim 3$  °C since 17.8 ky BP (Fig. 4B), in harmony with the prediction that hydrodynamic restriction should deliver cooler temperatures (6, 59), perhaps by as much as 4 to 6 °C. Hence, our  $\Delta_{47}$  support the notion that the Red Sea was more restricted than present during the last sea-level lowstand. However, t-tests of the  $\Delta_{47}$  data report no significant difference between the Holocene and Pleistocene at the 95% CI ([SI Appendix, Table S1](#)), supporting the hypothesis that the mesopelagic water mass in which our DWC specimens lived was not severely altered by the lowstand. Nor do the results of the Pettitt test find any

significant direction changes in the thermometry data at the 95% CI ([SI Appendix, Table S2](#)).

**Radiogenic Strontium.** Radiogenic strontium isotopes ( $^{87}\text{Sr}/^{86}\text{Sr}$ ) are believed to be homogeneously distributed in the global ocean because the residence time of strontium ( $10^6$  y) is  $>1,000\times$  the ocean mixing time (60, 61). Therefore, when the  $^{87}\text{Sr}/^{86}\text{Sr}$  ratio within a basin deviates from the global secular marine signal, it can be indicative of restriction. Once exchange between the basin and the global ocean is impeded, two primary mechanisms change the seawater  $^{87}\text{Sr}/^{86}\text{Sr}$  ratio: Riverine runoff and hydrothermal input. Both are relevant to the Red Sea (62, 63).

To establish the modern Red Sea  $^{87}\text{Sr}/^{86}\text{Sr}$  ratio, we measured 26 water samples. Our results, as well as those published by Kuznetsov et al. (64), indicate that the modern Red Sea is sufficiently connected to the Indian Ocean to maintain the global radiogenic strontium signature ( $0.709202 \pm 0.000003$ ). Additionally, our Late Holocene coral samples also have  $^{87}\text{Sr}/^{86}\text{Sr}$  ratios that are indistinguishable from modern (Fig. 4C), implying that their skeletons indeed record the  $^{87}\text{Sr}/^{86}\text{Sr}$  signature of seawater. If the Red Sea was meaningfully restricted during the last lowstand, we hypothesize that its corals would display  $^{87}\text{Sr}/^{86}\text{Sr}$  ratios that substantially differ from modern seawater.

To bound that hypothesis, we developed a box model to track the  $^{87}\text{Sr}/^{86}\text{Sr}$  ratio of seawater under the influence of ephemeral rivers (“wadis”) and hydrothermal vents ([SI Appendix, Fig. S2](#) and [Materials and Methods](#)). We contend these sources to be the dominant inputs of radiogenic strontium into an isolated Red Sea. That model advises that if the Red Sea were isolated from the Indian Ocean, the narrow bounds of the global  $^{87}\text{Sr}/^{86}\text{Sr}$  seawater signature ( $0.709202 \pm 0.000003$ , diagonal line [SI Appendix, Fig. S2](#)) could only be sustained through either negligible contribution from both hydrothermal and riverine inputs or a hydrothermal input twice that of the riverine flux ([SI Appendix, Fig. S2](#)). Developed in Discussion, we consider both scenarios unlikely.

Consider Fig. 4C which plots the  $^{87}\text{Sr}/^{86}\text{Sr}$  ratios of the corals versus their age. We frame these data against the range in the  $^{87}\text{Sr}/^{86}\text{Sr}$  ratio of modern Red Sea seawater which we measured (green envelope). A linear fit through those data advises their ratio to have increased between 18 ky BP and present by  $7e^{-6}$ . Monte Carlo analysis shows, however, that the  $^{87}\text{Sr}/^{86}\text{Sr}$  values of the Late Glacial corals are not significantly different from the Holocene ones ([SI Appendix, Table S1](#)).

While not definitive, our strontium data and box model suggest that even during the last sea-level lowstand, water exchange between the Indian Ocean and Red Sea must have been substantial. This is further supported by both the t-test and Pettitt tests. Neither report significant changes through time ([SI Appendix, Tables S1 and S2](#)).

**The  $\delta^{18}\text{O}$  Value of Coral Skeletons.** The  $\delta^{18}\text{O}$  value of coral carbonate ( $\delta^{18}\text{O}_{\text{CC}}$ ) is mediated by the vital effects of the organisms that precipitate it and by the  $\delta^{18}\text{O}$  values and temperature of the waters they inhabit (65). With regard to temperature, due to unknown vital effects in the studied species, we are agnostic to the notion that our  $\Delta_{47}$  thermometry data (Fig. 4B) inform on absolute Red Sea temperature but rather suppose they advise that its temperature was relatively stable over the last 18 ky. We therefore attribute the increase in the  $\delta^{18}\text{O}_{\text{CC}}$  values in the Late Glacial to an increase in evaporation rate relative to the exchange with the Indian Ocean, effectively concentrating  $\delta^{18}\text{O}$  values of the Red Sea ( $\delta^{18}\text{O}_{\text{RS}}$ ). The trend toward more negative  $\delta^{18}\text{O}_{\text{CC}}$  values during the Holocene is then consistent with increasing exchange between the Indian Ocean and Red Sea and the melting

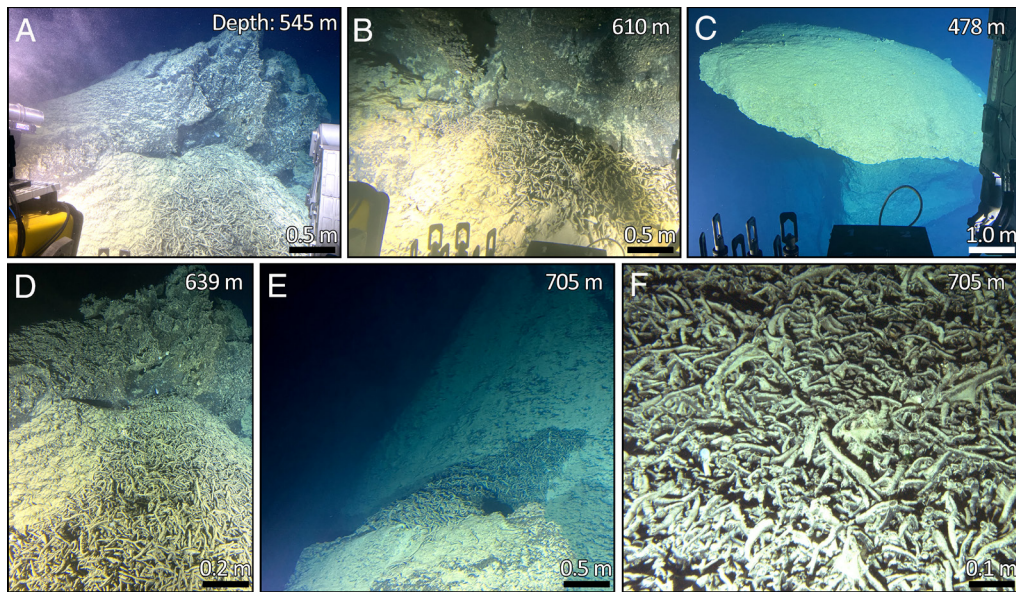


**Fig. 3.** *R. valida* death assemblages photographed during our submersible dives. Water depths and scales as noted. (A) and (B) show skeletons dissolving from cemented monospecific thickets of *R. valida* in life position and accumulating nearby on the seabed. (C) highlights the instability of the cements in modern seawater, with the underside of a fossil reef mound dissolved while the top is protected by a thin layer of hemipelagic mud. (D) and (E) depict skeletons accumulating several meters below the fossil mounds on steep slopes. (F) Close-up of one such accumulation.

of glacial ice caps. The  $\sim 1.2\%$  increase resulting from ice melt (66, 67) accounts for approximately 50% of the 2‰ change in  $\delta^{18}\text{O}_{\text{CC}}$  over 18 ky (red line, Fig. 4D). The Late Glacial  $\delta^{18}\text{O}_{\text{CC}}$  values are not significantly different to those from the Holocene (SI Appendix, Table S1). However, the  $\delta^{18}\text{O}_{\text{CC}}$  values become more negative around 6.5 ky BP, as noted by the Pettitt test (SI Appendix, Table S2).

Had the mesopelagic water mass occupied by our sampled DWCs suffered a lowstand salinity crisis, Late Glacial  $\delta^{18}\text{O}_{\text{RS}}$  values might have been more positive. Consider Hamelin Pool, for instance, a restricted embayment in Western Australia with a salinity double that of the open ocean and average  $\delta^{18}\text{O}$  values increased by +3.16 to +5.27‰ (68). If the Red Sea had been severely isolated during the last glacial lowstand, it might be reasonable to expect a far greater increase in the  $\delta^{18}\text{O}_{\text{RS}}$  values than evident in Fig. 4D.

## Discussion

**Continuous DWC Growth Since 18 ky.** Today, the Red Sea connects to the Indian Ocean via the 137-m deep Hanish Sill. The sill's depth may not have been constant since the last glacial lowstand due to active tectonics—it lies adjacent to the volcanically active Hanish Islands. Mitchell et al. (13), however, build a compelling case for only minor changes in sill topography back to the Mid Pleistocene. Therefore, the three sea-level curves shown in Fig. 4A likely inform on the connectivity between Red Sea and Indian Ocean since 20 ky BP.

*R. valida* skeletons were collected at 20 sites between 400 to 720 m water depth. So situated, these fossils resided sufficiently deep as to ensure they have not been subaerially exposed since the Pleistocene. At six additional sites, we sampled the mesophotic coral species *Leptoseris* between 80 and 90 m depth. Their skeletons returned dates between 0.8 and 7.8 ky BP. According to Fig. 4A, these samples also avoided subaerial exposure. If our fossils have undergone diagenesis, we are confident that it is only of the marine variety. This is relevant because diagenetic alteration by meteoric waters during subaerial exposure is disruptive to the U-Th ages and primary geochemical signals of coral carbonate.

U-Th geochronology returned coral ages ranging from 7.5 to 17.8 ky BP. Because the sea-level position during this timeframe is crucial for evaluating the extent of the Red Sea's restriction from the Indian Ocean, we compiled three sea-level curves (Fig. 4A) derived from various proxies across different geographic regions. At the broadest spatial extent, the curve of Lambeck et al. (36) charts global eustatic sea level. By including sea-level indicators from the Western Indian Ocean, Camoin et al. (37) provide a regional curve which better informs on the situation outside the Strait of Bab-el-Mandeb. Then, at the local scale, the curve from Siddall et al. (38) incorporates indicators from within the Red Sea basin.

All three studies agree that sea level was at least 110 m below present at the mean age of 17.8 ky BP for our oldest *R. valida* specimens. The record from Camoin et al. (37) suggests a slightly lower sea level at that time, around  $-115$  m. All three curves place the lowest sea level during the LGM near  $-120$  m, occurring around 20 ky BP. Sea level remained in this approximate range until the end of the LGM, which is commonly dated to 19 ky BP (11). Even when considering the 95% CI, which extend 488 years either side of the mean age of 17.8 ky BP for our oldest corals, the ages do not quite intercept the LGM. However, none of the curves suggest more than a 5 m change in sea level during the 2.2 ky interval between the lowest LGM lowstand at 20 ky BP and the mean ages of the corals. While the sea level was undoubtedly not static during this interval, determining its precise position falls outside the inherent uncertainties of sea-level reconstructions and the precision of U-Th dating. We propose that it is reasonable to conclude that our oldest coral specimens confirm that the Red Sea was inhabited during its period of maximum restriction. Indeed, all three sea-level curves suggest that the basin remained restricted until approximately 16.5 ky BP, when the main phase of deglaciation began (36), as also supported by the alkenone paleothermometry record of Arz et al. (6). That record reports Red Sea temperature to begin its rise back towards modern conditions at 16.5 ky BP. Even when accounting for the 95% CI around our mean ages, it is clear that the northern Red Sea supported live *R. valida* thickets before that time.

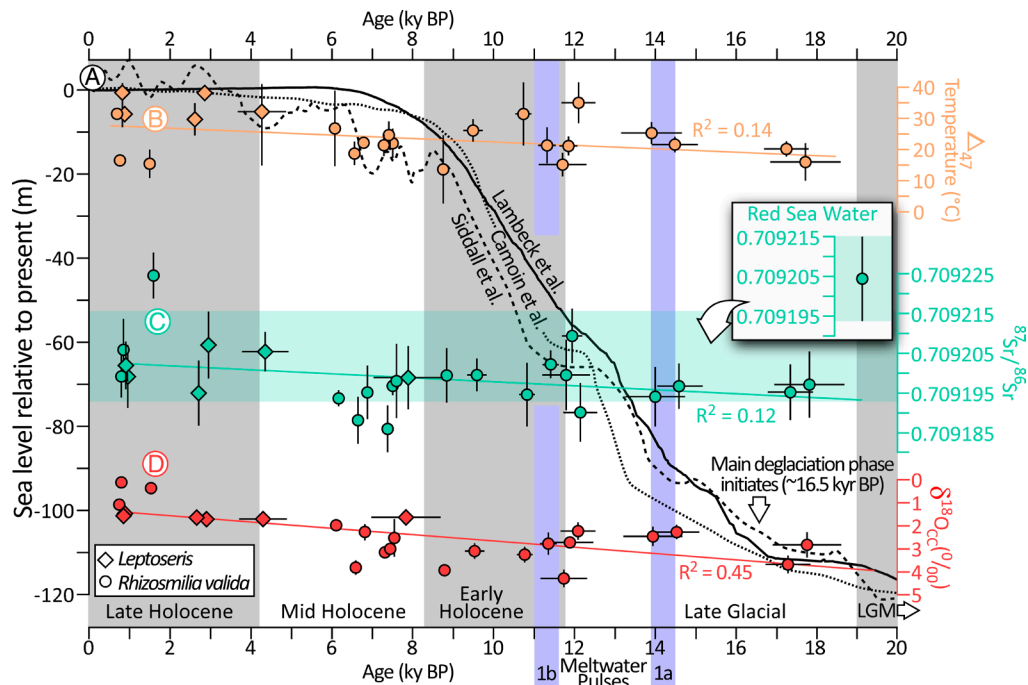


**Fig. 4.** Geochemistry of coral samples through time. (A) Sea-level changes since 20 ky BP, as reported by Lambeck et al. (36), Camoin et al. (37), and Siddall et al. (38) charted with 2.5-ky running means. Lambeck et al. (36) pins the major phase of deglaciation to initiate at approximately 16.5 ky BP. Timing of meltwater pulses 1a (~14.5 ky BP) and 1b (~11.2 ky BP) after Fairbanks et al. (55). (B) Clumped isotope ( $\Delta_{47}$ ) thermometry of the coral carbonate. (C)  $^{87}\text{Sr}/^{86}\text{Sr}$  ratios. (D)  $\delta^{18}\text{O}_{\text{CC}}$  values. Horizontal error bars represent 95% CI around mean Uranium-Thorium ages; vertical error bars, 95% CIs from triplicate geochemical measurements.

As DWCs are famed for their strong negative physiological response to even minor environmental perturbation, it is curious that they survived in a restricted basin, while planktonic organisms perished. Reports of Red Sea aplanktonic intervals hence deserve scrutiny.

**Do Red Sea Microfossils Support Basin-Wide Lowstand Extinction?** Fourteen Red Sea studies examining 27 deep-sea cores audit microfossils through the last sea-level minimum (Fig. 2). Their evidence for lethal basin-wide lowstand conditions is equivocal. If only planktonic forams are considered, a case could be made for lowstand extinction in the northern and central Red Sea. Plus, the lack of aplanktonic intervals in the northern Gulf of Aqaba and southern Red Sea might support the existence of glacial refugia in those locations (1, 12). Curiously, coccoliths, which inhabit surface waters like planktonic forams, were not extirpated during the LGM (MIS 2) or the Penultimate Glacial Period (MIS 6). Pteropods, which occupy the entire water column, and benthic forams, which live on the seabed, were similarly unaffected. Microfossil evidence suggests the lowstand Red Sea was not ecologically impoverished. Could the microfossil record be misinterpreted?

Restricted basins can respond swiftly and dramatically to minor events. Short-lived crises, lasting only decades to a century, might not manifest in a core. More pervasive crises should be apparent. To ensure quality, we selected only cores with an average sampling interval of 15 cm or finer (*Materials and Methods*). Misinterpretation of the microfossil record may also arise from seafloor remobilization by resuspension or gravity flows (31). Alternatively, given the prevailing circulation of surface waters (53, 69), calcareous shells of planktonic organisms from the Indian Ocean might drift into the lowstand Red Sea and deposit there, for instance, even if they could not survive there. We consider this unlikely. It would promote aplanktonic intervals in the north of the basin, which is far from the Indian Ocean connection, while dampening them in the south. This gradient is absent in the data (Fig. 2). Based upon the

available evidence, we therefore contend that our microfossil meta-analysis does not support basin-wide lowstand extinction due to hypersalinity. Indeed, the apparent survival of multiple microfossil groups through the last glacial lowstand does not contrast with our finding that corals inhabiting mesophotic and mesopelagic depths have grown in the basin for most of the last 18 ky. Yet, some caveats still persist, calling to be explored further.

**Geochemical Proxies Advocate for Normal Marine Conditions for Most of the Last 18 ky.** Multiple lines of geochemical evidence suggest the lowstand water mass occupied by the DWCs which we collected to not substantially differ from modern. To paleotemperature first. The Red Sea should cool if connection to the warm Indian Ocean is restricted (6, 59). Clumped isotope ( $\Delta_{47}$ ) thermometry data do not advise the temperature of the northern Red Sea to be significantly cooler prior to the main phase of deglaciation which initiated at 16.5 ky BP (36), than after it (Fig. 4B and *SI Appendix, Table S1*,  $P = 0.2$ ). Our findings differ from those of Arz et al. (6), who used alkenone paleothermometry to reconstruct temperatures in the region as being 4.2 °C cooler during the LGM, even 8.0 °C cooler around 16.5 ky BP. Their record was based on the alkenone-producing coccoliths *E. huxleyi* and *G. oceanica* which inhabit the photic zone. In contrast, our paleotemperature record is derived from DWCs which lived at much greater depths. Collectively, these observations suggest that the chilling of the surface water mass due to lowstand restriction may have been more severe than experienced at mesopelagic depth.

Second, we presume that carbonate precipitated by corals records the  $^{87}\text{Sr}/^{86}\text{Sr}$  ratio of the seawater in which they grow. Using a box model (*SI Appendix, Fig. S2*), we build a case for that ratio to markedly change if the Red Sea's hydrodynamic connection to the Indian Ocean was disrupted. Our model assumes that in isolation, the  $^{87}\text{Sr}/^{86}\text{Sr}$  ratio is influenced by input rivers and hydrothermal vents. Due to limited data, our model excludes the presumed minor contribution of aeolian dust as a potential radiogenic strontium source. Published  $^{87}\text{Sr}/^{86}\text{Sr}$  ratios for Red Sea

riverine waters range from 0.7108 to 0.7150 (70–73), considerably higher than the global ocean and modern Red Sea ( $0.709202 \pm 0.000003$ ). Riverine input to the basin would hence raise its radiogenic strontium value. Hydrothermal fluid ratios from the Red Sea (0.70702 to 0.70800) are lower than the global ocean (74–79). That source would lower the seawater ratio.

Box modeling suggests that Red Sea isolation from the Indian Ocean would only maintain the narrow global  $^{87}\text{Sr}/^{86}\text{Sr}$  seawater signature (diagonal line *SI Appendix*, Fig. S2) with either minimal hydrothermal and riverine inputs, or a hydrothermal flux double that of the riverine. The minimal input scenario is unlikely. The 10 ky duration of the last sea-level minimum (41) would seem ample to affect such changes. Could hydrothermal sources supply twice the radiogenic strontium of rivers?

While no perennial exorheic rivers flow into the modern Red Sea, winter rainfall triggers frequent flashfloods (80) and precipitation likely increased during glacial periods (26–31, 81). Although hydrothermal activity has been observed in the Red Sea, it remains limited (63); oceanic crust accretion is still in its early stages (82). Thus, hydrothermal strontium delivery is unlikely to outpace flashflood contributions by the needed factor of two.

Although we cannot entirely rule out that hydrothermal and riverine inputs, along with dust sources, may have maintained open-ocean  $^{87}\text{Sr}/^{86}\text{Sr}$  values in an isolated Red Sea, the most parsimonious expectation for a restricted Red Sea is a substantial change in the basin's radiogenic strontium signature. No such disruption is evident in the data (Fig. 4C).

Interpreting the temporal  $\delta^{18}\text{O}$  trend in our corals presents a particular challenge. In addition to temperature, these values change in response to the rate of evaporation of Red Sea water, to ice-sheet melting, and due to the vital effects of the corals themselves. We believe the effect of changing temperature of the Red Sea Intermediate Waters can largely be discounted due to its stability through time, as ascertained using clumped isotopes. Assuming our measured corals faithfully record the  $\delta^{18}\text{O}$  of the seawater in which they grew, the  $\sim 1\text{‰}$  ice-melt effect (66) might account for approximately half of the more negative trend reported in our corals since the LGM (Fig. 4D).

The remainder of that trend can reasonably be ascribed to increased evaporation from a semi-restricted lowstand Red Sea. Our Late Glacial DWCs do indeed show slightly more positive  $\delta^{18}\text{O}$  values compared to those from the Holocene, but the difference is insignificant (*SI Appendix*, Table S1). However, the Pettitt test found a statistically significant change in the  $\delta^{18}\text{O}$  data at about 6.5 ky BP (*SI Appendix*, Table S2), when the sea level reached its modern-day elevation and stabilized (Fig. 4A). Combining coccolith alkenones and  $\delta^{18}\text{O}$ , Arz et al. (6) estimated Red Sea surface-water paleosalinity to be approximately 50 PSU at the 17.8 ky BP mean age of our oldest *R. valida* skeletons. Values derived by Hemleben et al. (7) from the planktonic foram  $\delta^{18}\text{O}$  record pitch salinity to have reached 53 PSU. Modeling by Biton et al. (5) suggests a surface salinity value as high as 57 PSU.

Applying the evaporation model presented by Gonfiantini (83) (*Materials and Methods*), our  $\delta^{18}\text{O}$  data suggest a value of around 45 PSU at that time, after accounting for the ice-melt effect. While a direct comparison is not entirely appropriate—Arz et al., Hemleben et al., and Biton et al. analyzed a shallow water mass while our study focuses on a deeper one—both the shallow- and deep-water proxies consistently indicate that northern Red Sea lowstand paleosalinity was higher than the 40 PSU modern value at mesopelagic depth (31). Yet, salinity levels evidently remained within a range tolerated by DWCs, even when sea level stood low. While individual  $\Delta_{47}$ , radiogenic strontium, or  $\delta^{18}\text{O}$  values may not conclusively indicate that the mesopelagic Red Sea's temperature

and chemistry remained stable from the Late Glacial to the Holocene, the consistent support of all three proxies is compelling evidence for this conclusion.

## Conclusions

With a  $>110$  m sea-level fall at the end of the last glacial, the Red Sea has been hypothesized to have been drastically impacted, potentially to the point of basin-wide extinction. Contrary to this, our data suggest a more benign effect. DWCs grew during most of the Late Glacial period, showing no significant geochemical difference between the Late Glacial and Holocene. Meta-analysis of 27 cores indicates that while planktonic forams may have been locally extinct, other microfossil groups persisted. Our study presents a different perspective on the survival of Red Sea marine biota during the last sea-level lowstand. Evidence of DWC growth and reevaluation of core records point to a less drastic oceanographic situation. However, aspects such as the renewal of shallow-water benthic biota and the persistence of deep-sea benthos under challenging conditions remain unexplained. Our data suggest a more complex scenario than a simple on/off switch for viable conditions.

## Materials and Methods

**Submersible Sampling of Fossil Corals.** Fossil coral skeletons were sampled during submersible dives from the R/V OceanXplorer on research cruises in 2020, 2022, and 2023 (*SI Appendix*, Fig. S1). Two species were collected: the Red Sea endemic *R. valida* (Caryophylliidae) from 20 sites at depths of 400 to 720 m, and *Leptoseris* cf. *striatus* (Agariciidae) from six sites at depths of 80 to 90 m (Fig. 1). Note that Qurban et al. (51) identified *R. valida* as belonging to the genus *Dasmosmilia*. This species has since been reclassified as *Rhizosmilia* (84). Our 26 sample sites all situate south of the Tiran Straits, a tectonically active sill, 70 m deep at its minimum, which separates the Red Sea from the Gulf of Aqaba (85). So situated, this study cannot arbitrate the degree of additional restriction endured by the Gulf of Aqaba during the last sea-level lowstand, versus the Red Sea.

Fossil corals were found in two different settings. The first setting saw thickets of the fossil coral skeletons, cemented in life position, in a rock matrix. This matrix, though, is poorly lithified. The skeletons readily fall out of it as the matrix dissolves—delivering the second setting for the death assemblage. Here, the skeletons abundantly accumulate beneath the blocks from which they have fallen. Usually, these accumulations situate directly down-slope from their original position, but in the cases of a particularly steep slope, they might accumulate several meters away. The resultant piles of *R. valida* skeletons lightly re-cement in place. Due to limited strength of the manipulator arms on our submersibles, we exclusively collected the skeletons accumulating in this second scenario. We could exclude the possibility of postmortem transport of the coral skeletons which we sampled from shallower water depths by, for instance by earthquakes and/or turbidites, because the fossils lay so close to the original life-position thickets from which they had obviously been shed.

To avoid contamination, only the interior of the coral skeletons was sampled for geochemistry and geochronological analyses. The exterior was milled away using a rotary drill. The skeletons were then sonicated, rinsed multiple times with MilliQ water (18.2 M $\Omega$ -cm), and dried at 50 °C. Using a hand drill, 65 mg of powder was sampled from each skeleton and distributed for U-Th age dating, radiogenic strontium isotope analysis, clumped isotope analysis, stable isotope analysis of oxygen, and trace metal concentrations.

**U-Th Geochronology of Coral Skeletons.** The chronology of all fossil coral samples was established using U-Th geochronometry at the U. Miami Neptune Isotope Lab. Approximately 35 mg of powdered skeleton was dissolved in 5 ml of 0.45 mol l<sup>-1</sup> HNO<sub>3</sub> and filtered through a 0.22- $\mu\text{m}$  PFA filter. The samples were spiked with a mixture of  $^{229}\text{Th}/^{233}\text{U}/^{236}\text{U}$  and equilibrated for Isotope Dilution Mass Spectrometry. The molarity of the filtrate was adjusted to  $>6$  mol l<sup>-1</sup> HNO<sub>3</sub> using distilled high-purity nitric acid to ensure quantitative separation of U and Th from matrix elements using established U/TEVA (Eichrom™) extraction chromatography. The elution aliquots containing purified U and Th were evaporated overnight at

70 °C and dissolved in a 0.45 mol l<sup>-1</sup> HNO<sub>3</sub> and 0.1 mol l<sup>-1</sup> HF mixture. The U and Th isotopes were analyzed in separate sessions on a Neptune Plus MC-ICPMS.

The U-Th ages were calculated using an Algorithm in Mathematica assuming initial <sup>230</sup>Th/<sup>232</sup>Th activity ratio of 0.6 ± 0.2 to account for detrital (excess) <sup>230</sup>Th. Choosing larger values does not impact the age adjustment significantly because the analyzed corals contained low levels of the common <sup>232</sup>Th. For additional details regarding extraction chromatography, isotope mass spectrometry, and U-Th age calculation and uncertainty propagation, see Pourmand et al. (86).

**Modern Red Sea Water Samples.** We sampled the seawater at the same sites where we collected coral skeletons using 1.5-liter Niskin bottles mounted on two Triton submersibles. Hence, 26 water samples in total. The seawater in each Niskin was subsampled into 2 ml aliquots, passed through a 0.45 μm filter, and the molarity of the seawater adjusted to 6 mol l<sup>-1</sup> HNO<sub>3</sub> using distilled high-purity nitric acid. We then determined the <sup>87</sup>Sr/<sup>86</sup>Sr ratio of seawater subsamples using the same methodology as used for the coral skeletons—see below.

**Radiogenic Strontium Ratios of Coral and Seawater Samples.** We determined the radiogenic strontium isotopic composition of seawater samples and coral skeletons from the Red Sea. Extraction of Sr from matrix elements was achieved using the Sr resin (Eichrom™) following established procedures (86). Every five measurements were bracketed with wash solutions and certified reference materials, SRM987. The measured <sup>87</sup>Sr/<sup>86</sup>Sr ratio of the standard was 0.710273 ± 0.000007 (n = 21). The values we report are not adjusted to this standard but are corrected for instrumental mass-bias and isobaric interference (86).

**Restricted Red Sea Radiometric Strontium Box Model.** We hypothesize that prolonged isolation during the last glacial lowstand would give Red Sea corals distinct <sup>87</sup>Sr/<sup>86</sup>Sr ratios from the global ocean. To evaluate this hypothesis, we developed a box model simulating the temporal evolution of strontium isotopic composition in an isolated Red Sea. The model used a fixed Red Sea volume of 2.25 × 10<sup>14</sup> m<sup>3</sup> (87) and incorporated strontium inputs from two sources (SI Appendix, Fig. S2). The first was ephemeral rivers. Based on estimates from literature, we considered ephemeral riverine fluxes ranging from negligible values up to 0.5 × 10<sup>9</sup> kg/y (53). This range reflects the arid climate and lack of perennial exorheic rivers in the region. We assigned an isotopic value of 0.71271 to the riverine flux, reflecting the average <sup>87</sup>Sr/<sup>86</sup>Sr values reported for rivers in the region. (70–73).

The second input in our box model was hydrothermal vent flux, which is not well-characterized in the Red Sea. We therefore used a range of values from 0 to 0.5 × 10<sup>9</sup> kg/y, assigning an <sup>87</sup>Sr/<sup>86</sup>Sr value of 0.707498 based on the average of measured hydrothermal values in the basin (74–79). We set the initial strontium concentration to 0.0082 (88), reflecting modern global ocean levels, and an initial isotopic value of 0.709202, based on our measurements of Red Sea seawater (Fig. 4C).

Our model assumed no exchange with the Indian Ocean and maintained a constant strontium concentration throughout the run. It was executed with a 10-year timestep over a 10,000-year period, representing the duration of the last glacial sea-level minimum (41). The following differential equation describes the total strontium mass balance of the system

$$\frac{dM_{Sr}}{dt} = F_{river} + F_{hydro} - kM_{Sr}$$

where  $M_{Sr}$  is the total mass of strontium in the Red Sea (kg) calculated based on the initial concentration of Sr and the volume of the Red Sea,  $F_{river}$  is the riverine strontium flux (kg/y),  $F_{hydro}$  is the hydrothermal strontium flux (kg/y), and  $k$  is the removal rate constant (y<sup>-1</sup>), representing strontium removal via sedimentation, which is calculated independently for each combination of  $F_{river}$  and  $F_{hydro}$  to keep the concentration of strontium constant throughout the simulation.

The isotopic composition balance in the model was then set according to

$$\frac{d(RM_{Sr})}{dt} = R_{river}F_{river} + R_{hydro}F_{hydro} - kRM_{Sr}$$

where  $R$  is the <sup>87</sup>Sr/<sup>86</sup>Sr in the Red Sea at time  $t$ .  $R_{river}$  and  $R_{hydro}$  are the isotopic ratios of the riverine and hydrothermal inputs.

**Elemental and Mineral Analysis of Coral Skeletons.** The mineralogy of each coral was determined by dissolving 2.5 mg of its powdered skeleton in 10 ml of 4% OMNI TRACE HNO<sub>3</sub>. Concentrations of Ca, Sr, and Mg in this solute were measured on a Varian Vista Pro Inductively Coupled Plasma-Optical Emission Spectrometer (ICP-OES) and calibrated using matrix-matched standards. We report our data as Sr/Ca and Mg/Ca ratios in mmol/mol. This workflow has been ascertained to deliver precision <1% (89, 90).

**Clumped Isotope Thermometry and δ<sup>18</sup>O of Coral Skeletons.** Despite their vital effects, corals have been widely used to ascertain past variations in temperature as well as changes in the δ<sup>18</sup>O values of their environment (91). We determined the Δ<sub>47</sub> and δ<sup>18</sup>O values of the coral skeletons using a Thermo 253-Plus MS using standard methods (92, 93). The δ<sup>18</sup>O values are reported relative to the Vienna Pee Dee Belemnite (VPDB) (94) in the normal convention and have been corrected for the usual isobaric interference (95). All samples were analyzed in triplicate. The Δ<sub>47</sub> values were corrected using both the CO<sub>2</sub> equilibrated (CDES) (96) and the Intercarb CDES (I-CDES) scales (58). As the differences between these correction schemes is <10 ppm and is typically less than the shot noise of the measurement as calculated using the approach of Merrit et al. (97), we have used the CDES values for consistency with our previous analyses. As there were small amounts of calcite in most of the coral samples analyzed, we used the Sr/Ca ratio of the samples to estimate the percentage of calcite and original aragonite in each sample (Dataset S1). We also used the observation of Saenger et al. (98) that Scleractinian corals form their skeletons with slightly more positive Δ<sub>47</sub> values (equal to about 8 °C) than expected from equilibrium. Assuming that the calcite in the skeleton formed in approximate equilibrium to the temperature in which the coral grew, the temperature could be calculated using the relationship of Swart et al. (93).

The salinity of the seawater in which the corals lived could also be reconstructed based on the δ<sup>18</sup>O of their skeletons (SI Appendix, Fig. S3). Here, we applied the evaporation model of Gonfiantini (83) using an initial salinity for northern Red Sea mesopelagic seawater of 40 PSU (31), a coral carbonate δ<sup>18</sup>O value of +1‰, a δ<sup>18</sup>O value of atmospheric water vapor in approximate isotopic equilibrium with the surface water, a temperature of 25 °C, and a relative humidity of 75%. These values are equivalent to the current average conditions in the Red Sea.

#### Error Estimation and Statistical Treatment of Coral Geochemistry Results.

To assess whether the geochemistry of corals which inhabited mesopelagic water depths during the last glacial lowstand differs statistically from those after the sea level rose, we divided our samples into two age groups. The first group included seven Late Glacial corals (older than 11.7 ky BP) and the second group consisted of 19 Holocene-aged corals. Recognizing the limited dataset size, we employed a Monte Carlo resampling method to test robustness. Each geochemical measurement was resampled from a normal distribution based on its original mean and SD. We conducted t-tests on each resampled dataset and repeated this simulation 10,000 times to determine statistical significance (SI Appendix, Table S1). We also conducted Pettitt tests on each dataset to determine the change-point direction (99) (SI Appendix, Table S2). This test identifies the years there is a statistically significant shift in the data's overall trend.

**Meta-Analysis of Red Sea Planktonic Intervals.** The disappearance of planktonic organisms during sea-level lowstands suggests that Red Sea restriction is catastrophic for its biota. Several studies examining a total of 27 cores have audited the presence/absence of forams, pteropods, and coccolithophores through the last glacial lowstand. We summarize these data to evaluate the evidence for and against the notion that the Red Sea dies during sea-level minima. Each core included in our meta-analysis met three criteria: 1) Data were published and publicly accessible, 2) an accompanying age model was available, and 3), by means of quality control, microfossils were audited for at an average sampling frequency of 15 cm or finer. To avoid bias in our meta-analysis, we applied a consistent ecological presence/absence methodology to the published microfossil records. Specifically, any reported presence of a microfossil in a given core horizon was marked as "present" in our analysis, while "absence" was only assigned to core horizons with zero microfossil counts. Our meta-analysis results are presented in Dataset S1 and as a map showing each core's location, the persistence of microfossils through time, and the frequency with which each core was sampled (Fig. 2).

**Data, Materials, and Software Availability.** All study data are included in the article and/or supporting information.

**ACKNOWLEDGMENTS.** We owe a debt of gratitude to our Saudi Arabian partners, NEOM, and to Richard Bush, Deborah Colbourne, Jennifer Munro, and Abdulqader Khamis for their support. We are also indebted to OceanX and the crew of OceanXplorer for their operational and logistical assistance. Special thanks to Andrew Craig, Olaf Dieckhoff, Ewan Bason, and Kate von Krusenstern for data acquisition, sample collection, and support of scientific operations aboard OceanXplorer. We also thank OceanX Media for documenting and communicating this work to the public. Gratitude is extended to Mike Ackerman for assistance with sample preparation. We sincerely thank the three anonymous reviewers for their

thoughtful and constructive feedback which improved the clarity and depth of our manuscript. This is Ismar-CNR, Bologna, scientific contribution no. 2095. This study was funded by NEOM Agreement No: SRA-ENV-2023-001/AWD-008854 to the University of Miami.

Author affiliations: <sup>a</sup>Department of Marine Geosciences, Rosenstiel School of Marine, Atmospheric, and Earth Science, University of Miami, Miami, FL 33149; <sup>b</sup>Beta Analytic Inc., Isobar Science, Miami, FL 33155; <sup>c</sup>Red Sea Research Center, King Abdullah University of Science and Technology, Thuwal 23955, Saudi Arabia; <sup>d</sup>The Isotoparium, Division of Geological and Planetary Sciences, California Institute of Technology, Pasadena, CA 91125; <sup>e</sup>Istituto di Scienze Marine (CNR-ISMAR), Bologna I-40129, Italy; <sup>f</sup>Stazione Zoologica "Anton Dohrn", Napoli I-80121, Italy; and <sup>g</sup>OceanX, New York, NY 10018

1. S. Locke, R. C. Thunell, Paleocceanographic record of the last glacial/interglacial cycle in the Red Sea and Gulf of Aden. *Paleoceanogr. Paleoclimatol. Paleocool.* **64**, 163–187 (1988).
2. R. C. Thunell, S. M. Locke, D. F. Williams, Glacio-eustatic sea-level control on Red Sea salinity. *Nature* **334**, 601–604 (1988).
3. P. Hofmann *et al.*, "Sedimentation, organic geochemistry and diagenesis of cores from the axial zone of the southern Red Sea: Relationships to rift dynamics and climate" in *Sedimentation and Tectonics in Rift Basins Red Sea: Gulf of Aden*, (Springer, 1998), pp. 479–504.
4. E. J. Rohling, Paleosalinity: Confidence limits and future applications. *Mar. Geol.* **163**, 1–11 (2000).
5. E. Biton, H. Gildor, W. Peltier, Red Sea during the Last Glacial Maximum: Implications for sea level reconstruction. *Paleoceanography* **23**, PA1214 (2008).
6. H. W. Arz, J. Pätzold, P. J. Müller, M. O. Moammar, Influence of Northern Hemisphere climate and global sea level rise on the restricted Red Sea marine environment during termination I. *Paleoceanography* **18**, 1053 (2003).
7. C. Hemleben *et al.*, Three hundred eighty thousand year long stable isotope and faunal records from the Red Sea: Influence of global sea level change on hydrography. *Paleoceanography* **11**, 147–156 (1996).
8. Z. Reiss *et al.*, Late Quaternary paleoceanography of the Gulf of Aqaba (Elat), Red Sea. *Quat. Res.* **14**, 294–308 (1980).
9. A. Almogi-Labin, Stratigraphic and paleoceanographic significance of Late Quaternary pteropods from deep-sea cores in the Gulf of Aqaba (Elat) and northernmost Red Sea. *Mar. Micropaleontol.* **7**, 53–72 (1982).
10. E. Ivanova, Late Quaternary biostratigraphy and paleotemperatures of the Red Sea and the Gulf of Aden based on planktonic foraminifera and pteropods. *Mar. Micropaleontol.* **9**, 335–364 (1985).
11. P. U. Clark *et al.*, The last glacial maximum. *Science* **325**, 710–714 (2009).
12. M. Fenton, S. Geiselhart, E. Rohling, C. Hemleben, Planktonic zones in the Red Sea. *Mar. Micropaleontol.* **40**, 277–294 (2000).
13. N. C. Mitchell, M. Ligi, E. J. Rohling, Red Sea isolation history suggested by Plio-Pleistocene seismic reflection sequences. *Earth Planet. Sci. Lett.* **430**, 387–397 (2015).
14. J. D. Milliman, D. A. Ross, T.-L. Ku, Precipitation and lithification of deep-sea carbonates in the Red Sea. *J. Sediment. Res.* **39**, 724–736 (1969).
15. M. Taviani, "Stable tropics not so stable: Climatically driven extinctions of reef-associated molluscan assemblages (Red Sea and Western Indian Ocean; Last interglaciation to present)" in *Reefs and Carbonate Platforms in the Pacific and Indian Oceans*, G. F. Camoin, P. J. Davies, Eds. (International Association of Sedimentologists, 1998), vol. 25, pp. 69–76.
16. A. Almogi-Labin, C. Hemleben, D. Meischner, H. Erlenkeuser, Paleoenvironmental events during the last 13,000 years in the central Red Sea as recorded by pteropoda. *Paleoceanography* **6**, 83–98 (1991).
17. M. Taviani, "Axial sedimentation of the Red Sea transitional region (22–25 N): Pelagic, gravity flow and sapropel deposition during the late quaternary" in *Sedimentation and Tectonics in Rift Basins Red Sea: Gulf of Aden*, (Springer, 1998), pp. 467–478.
18. W. Klauswitz, Evolutionary history and zoogeography of the Red Sea ichthyofauna. *Fauna of Saudi Arabia* **10**, 310 (1989).
19. G. Gvirtzman *et al.*, Morphology of the Red Sea fringing reefs a result of the erosional pattern of the last-glacial low-stand sea level and the following Holocene recolonization. *Bureau Recherches Géologiques et Minières (France)* **89**, 480–491 (1977).
20. M. Taviani *et al.*, Last glacial deep-water corals from the Red Sea. *Bull. Mar. Sci.* **81**, 361–370 (2007).
21. R. d. C. Portilho-Ramos *et al.*, Major environmental drivers determining life and death of cold-water corals through time. *PLoS Biol.* **20**, e3001628 (2022).
22. H. G. Fink *et al.*, Oxygen control on Holocene cold-water coral development in the eastern Mediterranean Sea. *Deep Sea Res. Part I: Oceanogr. Res. Papers* **62**, 89–96 (2012).
23. J. D. DiBattista *et al.*, On the origin of endemic species in the Red Sea. *J. Biogeogr.* **43**, 13–30 (2016).
24. T. I. Terraneo, F. Benzioni, R. Arrigoni, M. L. Berumen, Species delimitation in the coral genus *Goniopora* (Scleractinia, Poritidae) from the Saudi Arabian Red Sea. *Mol. Phylogenet. Evol.* **102**, 278–294 (2016).
25. S. V. Bogorodsky, J. E. Randall, "Endemic Fishes of the Red Sea" in *Oceanographic and Biological Aspects of the Red Sea*, N. M. A. Rasul, I. C. F. Stewart, Eds. (Springer International Publishing, Cham, 2019), [https://doi.org/10.1007/978-3-319-99417-8\\_14](https://doi.org/10.1007/978-3-319-99417-8_14), pp. 239–265.
26. G. de Lattin, Grundriss der zoogeographie (G. Fischer, 1967), vol. **12**.
27. B. Gabriel, "Klima- und landschaftswandel der Sahara." in *Sahara. 10000 Jahre zwischen weide und wüste*, P. Stehli, Ed. (Handbuch zu einer Ausstellung des Rautenstrauch-Joest-Museums für Volkerkunde, Kolon, 1978), pp. 22–34.
28. D. Fleitmann *et al.*, Holocene forcing of the Indian monsoon recorded in a stalagmite from southern Oman. *Science* **300**, 1737–1739 (2003).
29. J. A. Rech, J. Pigati, M. Al Kuisi, J. Bright, "The rise and fall of late Pleistocene paleolakes in southern Jordan" in *Geol. Soc. Am. Abstracts Programs* (2013), p. 680.
30. A. Parton *et al.*, Alluvial fan records from southeast Arabia reveal multiple windows for human dispersal. *Geology* **43**, 295–298 (2015).
31. S. J. Purkis *et al.*, Discovery of the deep-sea NEOM Brine Pools in the Gulf of Aqaba, Red Sea. *Commun. Earth Environ.* **3**, 146 (2022).
32. S. J. Purkis, G. Rowlands, B. Riegl, P. Renaud, The paradox of tropical karst morphology in the coral reefs of the arid Middle East. *Geology* **38**, 227–230 (2010).
33. E. J. Rohling, K. M. Grant, A. P. Roberts, J.-C. Larrasoana, Paleoclimate variability in the Mediterranean and Red Sea regions during the last 500,000 years: Implications for hominin migrations. *Curr. Anthropol.* **54**, S183–S201 (2013).
34. S. L. Nicholson *et al.*, Pluvial periods in Southern Arabia over the last 1.1 million-years. *Quater. Sci. Rev.* **229**, 106112 (2020).
35. G. N. Bailey *et al.*, Coastlines, submerged landscapes, and human evolution: The Red Sea basin and the Farasan Islands. *J. Island Coast. Archaeol.* **2**, 127–160 (2007).
36. K. Lambeck, H. Rouby, A. Purcell, Y. Sun, M. Sambridge, Sea level and global ice volumes from the Last Glacial Maximum to the Holocene. *Proc. Natl. Acad. Sci. U.S.A.* **111**, 15296–15303 (2014).
37. G. Camoin, L. Montaggioni, C. Braithwaite, Late glacial to post glacial sea levels in the Western Indian Ocean. *Mar. Geol.* **206**, 119–146 (2004).
38. M. Siddall *et al.*, Sea-level fluctuations during the last glacial cycle. *Nature* **423**, 853–858 (2003).
39. K. Lambeck *et al.*, Sea level and shoreline reconstructions for the Red Sea: Isostatic and tectonic considerations and implications for hominin migration out of Africa. *Quater. Sci. Rev.* **30**, 3542–3574 (2011).
40. K. Grant *et al.*, Rapid coupling between ice volume and polar temperature over the past 150,000 years. *Nature* **491**, 744–747 (2012).
41. W. Peltier, R. G. Fairbanks, Global glacial ice volume and Last Glacial Maximum duration from an extended Barbados sea level record. *Quater. Sci. Rev.* **25**, 3322–3337 (2006).
42. A. Winter *et al.*, Salinity tolerance or marine organisms deduced from Red Sea Quaternary record. *Mar. Geol.* **53**, M17–M22 (1983).
43. H. L. Legge, J. Mutterlose, H. W. Arz, Climatic changes in the northern Red Sea during the last 22,000 years as recorded by calcareous nannofossils. *Paleoceanography* **21**, PA1003 (2006).
44. H.-L. Legge, J. Mutterlose, H. W. Arz, J. Pätzold, Nannoplankton successions in the northern Red Sea during the last glaciation (60 to 14.5 ka BP): Reactions to climate change. *Earth Planet. Sci. Lett.* **270**, 271–279 (2008).
45. E. Rohling *et al.*, Sea-level and deep-sea-temperature variability over the past 5.3 million years. *Nature* **508**, 477–482 (2014).
46. A. Badawi, G. Schmiedl, C. Hemleben, Impact of late Quaternary environmental changes on deep-sea benthic foraminiferal faunas of the Red Sea. *Mar. Micropaleontol.* **58**, 13–30 (2005).
47. A. Almogi-Labin, B. Luz, J.-C. Duplessy, Quaternary paleo-oceanography, pteropod preservation and stable-isotope record of the Red Sea. *Paleoceanogr. Paleoclimatol. Paleocool.* **57**, 195–211 (1986).
48. A. Almogi-Labin, C. Hemleben, D. Meischner, Carbonate preservation and climatic changes in the central Red Sea during the last 380 kyr as recorded by pteropods. *Mar. Micropaleontol.* **33**, 87–107 (1998).
49. W. A. Berggren, A. Boersma, "Late Pleistocene and Holocene Planktonic Foraminifera from the Red Sea" in *Hot Brines and Recent Heavy Metal Deposits in the Red Sea: A Geochemical and Geophysical Account*, E. T. Degens, D. A. Ross, Eds. (Springer Berlin Heidelberg, Berlin, Heidelberg, 1969), pp. 282–298.
50. C. Chen, "Pteropods in the Hot Brine Sediments of the Red Sea" in *Hot Brines and Recent Heavy Metal Deposits in the Red Sea: A Geochemical and Geophysical Account*, E. T. Degens, D. A. Ross, Eds. (Springer Berlin Heidelberg, Berlin, Heidelberg, 1969), pp. 313–316.
51. M. A. Qurban *et al.*, In-situ observation of deep water corals in the northern Red Sea waters of Saudi Arabia. *Deep Sea Res. Part I: Oceanogr. Res. Papers* **89**, 35–43 (2014).
52. G. Scheer, C. G. Pillai, Report on the stony corals from the Red Sea. *Zoologica* **45**, 1–198 (1983).
53. S. S. Sofianos, W. E. Johns, An oceanic general circulation model (OGCM) investigation of the Red Sea circulation: 2. Three-dimensional circulation in the Red Sea. *J. Geophys. Res. [Oceans]* **108** (2003).
54. S. Fallon, R. Thresher, J. Adkins, Age and growth of the cold-water scleractinian *Solenosmilia variabilis* and its reef on SW Pacific seamounts. *Coral Reefs* **33**, 31–38 (2014).
55. R. G. Fairbanks, C. D. Charles, J. D. Wright, "Origin of global meltwater pulses" in *Radiocarbon after four decades: An interdisciplinary perspective* (Springer, 1992), pp. 473–500.
56. Z. Wang, E. A. Schauble, J. M. Eiler, Equilibrium thermodynamics of multiply substituted isotopologues of molecular gases. *Geochim. Cosmochim. Acta* **68**, 4779–4797 (2004).
57. P. Ghosh *et al.*, <sup>13</sup>C-<sup>18</sup>O bonds in carbonate minerals: A new kind of paleothermometer. *Geochim. Cosmochim. Acta* **70**, 1439–1456 (2006).
58. S. M. Bernasconi *et al.*, InterCarb: A community effort to improve interlaboratory standardization of the carbonate clumped isotope thermometer using carbonate standards. *Geochim. Geophys. Geosys.* **22**, e2020GC009588 (2021).
59. E. Halicz, Z. Reiss, Paleocological relations of foraminifera in a desert-enclosed sea—The Gulf of Aqaba (Elat), Red Sea. *Mar. Ecol. Prog. Ser.* **2**, 15–34 (1981).
60. G. Faure, *Principles of isotope geology* (Wiley, New York, 1977).
61. J. M. McArthur, Recent trends in strontium isotope stratigraphy. *Terra Nova* **6**, 331–358 (1994).
62. H. W. Arz, F. Lamy, J. Pätzold, P. J. Müller, M. Prins, Mediterranean moisture source for an early-Holocene humid period in the northern Red Sea. *Science* **300**, 118–121 (2003).
63. F. M. Van der Zwan *et al.*, Widespread diffuse venting and large microbial iron-mounds in the Red Sea. *Commun. Earth Environ.* **4**, 496 (2023).
64. A. Kuznetsov, M. Semikhatov, I. Gorokhov, The Sr isotope composition of the world ocean, marginal and inland seas: Implications for the Sr isotope stratigraphy. *Stratigr. Geol. Correlat.* **20**, 501–515 (2012).



65. J. N. Weber, P. M. Woodhead, Temperature dependence of oxygen-18 concentration in reef coral carbonates. *J. Geophys. Res.* **77**, 463–473 (1972).
66. D. Schrag, D. DePaolo, Determination of  $\delta^{18}\text{O}$  of seawater in the deep ocean during the Last Glacial Maximum. *Paleoceanography* **8**, 1–6 (1993).
67. J.-C. Duplessy, Isotope studies. *Clim. Change* **3**, 47–67 (1978).
68. S. P. Ahearn, *A Geochemical Description of Shark Bay's Hamelin Pool* (University of Miami, WA, 2019).
69. S. S. Sofianos, W. E. Johns, An oceanic general circulation model (OGCM) investigation of the Red Sea circulation, 1. Exchange between the Red Sea and the Indian Ocean. *J. Geophys. Res. [Oceans]* **107**, 17–11 (2002).
70. P. Boger, G. Faure, Strontium-isotope stratigraphy of a Red Sea core. *Geology* **2**, 181–183 (1974).
71. D. Bosch, J. Lancelot, J. Boulegue Sr., Nd and Pb isotope constraints on the formation of the metalliferous sediments in the Nereus Deep, Red Sea. *Earth Planet. Sci. Lett.* **123**, 299–315 (1994).
72. E. Hegner, J. Pallister, Pb, Sr, and Nd isotopic characteristics of Tertiary Red Sea Rift volcanics from the central Saudi Arabian coastal plain. *J. Geophys. Res.: Solid Earth* **94**, 7749–7755 (1989).
73. D. Palchan *et al.*, Synoptic conditions of fine-particle transport to the last interglacial Red Sea-Dead Sea from Nd-Sr compositions of sediment cores. *Quat. Sci. Rev.* **179**, 123–136 (2018).
74. G. Faure, L. M. Jones, "Anomalous Strontium in the Red Sea Brines" in *Hot Brines and Recent Heavy Metal Deposits in the Red Sea: A Geochemical and Geophysical Account*, E. T. Degens, D. A. Ross, Eds. (Springer Berlin Heidelberg, Berlin, Heidelberg, 1969), pp. 243–250.
75. R. Carwile, G. Faure, Strontium isotope ratios and base metal content in a core from the Atlantis II deep, Red Sea. *Chem. Geol.* **8**, 15–23 (1971).
76. M. Ikpeama, P. Boger, G. Faure, A study of strontium in core 119K, Discovery Deep, Red Sea. *Chem. Geol.* **13**, 11–22 (1974).
77. R. Zierenberg, W. C. Shanks III, Isotopic constraints on the origin of the Atlantis II, Suakin and Valdivia brines, Red Sea. *Geochim. Cosmochim. Acta* **50**, 2205–2214 (1986).
78. P. Anschutz, G. Blanc, Heat and salt fluxes in the Atlantis II Deep (Red Sea). *Earth Planet. Sci. Lett.* **142**, 147–159 (1996).
79. M. Stein, A. Almogi-Labin, S. L. Goldstein, C. Hemleben, A. Starinsky, Late Quaternary changes in desert dust inputs to the Red Sea and Gulf of Aden from  $^{87}\text{Sr}/^{86}\text{Sr}$  ratios in deep-sea cores. *Earth Planet. Sci. Lett.* **261**, 104–119 (2007).
80. T. Katz *et al.*, Desert flash floods form hyperpycnal flows in the coral-rich Gulf of Aqaba, Red Sea. *Earth Planet. Sci. Lett.* **417**, 87–98 (2015).
81. T. Felis *et al.*, Increased seasonality in Middle East temperatures during the last interglacial period. *Nature* **429**, 164–168 (2004).
82. J. Gaulier *et al.*, Seismic study of the crust of the northern Red Sea and Gulf of Suez. *Tectonophysics* **153**, 55–88 (1988).
83. R. Gonfiantini, "Environmental isotopes in lake studies" in *Handbook of Environmental Isotope Geochemistry, The Terrestrial Environment*, B. P. Fritz, J. C. Fontes, Eds. (Elsevier, Amsterdam, 1986), pp. 113–168.
84. B. Hoeksema, S. Cairns, World list of Scleractinia. (2019), <http://www.marinespecies.org/aphia.php>.
85. S. J. Purkis *et al.*, Tsunamiogenic potential of an incipient submarine landslide in the Tiran Straits. *Geophys. Res. Lett.* **49**, e2021GL097493 (2022).
86. A. Pourmand, F. L. Tissot, M. Arienzo, A. Sharifi, Introducing a comprehensive data reduction and uncertainty propagation algorithm for U-Th geochronometry with extraction chromatography and isotope dilution MC-ICP-MS. *Geostand. Geoanal. Res.* **38**, 129–148 (2014).
87. Y. Chung, R. Finkel, K. Kim,  $^{226}\text{Ra}$ ,  $^{210}\text{Pb}$  and  $^{210}\text{Po}$  in the Red Sea. *Earth Planet. Sci. Lett.* **58**, 213–224 (1982).
88. M. Lebrato *et al.*, Global variability in seawater Mg: Ca and Sr: Ca ratios in the modern ocean. *Proc. Natl. Acad. Sci. U.S.A.* **117**, 22281–22292 (2020).
89. B. E. Rosenheim, P. K. Swart, S. R. Thorold, Minor and trace elements in sclerosponge *Ceratoporella nicholsoni*: Biogenic aragonite near the inorganic endmember? *Palaeogeogr. Palaeoclimatol. Palaeoecol.* **228**, 109–129 (2005).
90. S. J. Giri, P. K. Swart, Q. B. Devlin, The effect of changing seawater Ca and Mg concentrations upon the distribution coefficients of Mg and Sr in the skeletons of the scleractinian coral *Pocillopora damicornis*. *Geochim. Cosmochim. Acta* **222**, 535–549 (2018).
91. A. G. Grottoli, C. M. Eakin, A review of modern coral  $\delta^{18}\text{O}$  and  $\Delta^{14}\text{C}$  proxy records. *Earth Sci. Rev.* **81**, 67–91 (2007).
92. S. T. Murray, M. M. Arienzo, P. K. Swart, Determining the  $\Delta_{47}$  acid fractionation in dolomites. *Geochim. Cosmochim. Acta* **174**, 42–53 (2016).
93. P. K. Swart, S. T. Murray, P. T. Staudigel, D. A. Hodell, Oxygen isotopic exchange between  $\text{CO}_2$  and phosphoric acid: Implications for the measurement of clumped isotopes in carbonates. *Geochim. Geophys. Res.* **20**, 3730–3750 (2019).
94. I. Friedman, J. O'Neil, G. Cebula, Two new carbonate stable-isotope standards. *Geostandards Newsletter* **6**, 11–12 (1982).
95. H. Craig, Isotopic standards for carbon and oxygen and correction factors for mass-spectrometric analysis of carbon dioxide. *Geochim. Cosmochim. Acta* **12**, 133–149 (1957).
96. K. J. Dennis, H. P. Affek, B. H. Passey, D. P. Schrag, J. M. Eiler, Defining an absolute reference frame for 'clumped' isotope studies of  $\text{CO}_2$ . *Geochim. Cosmochim. Acta* **75**, 7117–7131 (2011).
97. D. A. Merritt, J. Hayes, Factors controlling precision and accuracy in isotope-ratio-monitoring mass spectrometry. *Anal. Chem.* **66**, 2336–2347 (1994).
98. C. Saenger *et al.*, Carbonate clumped isotope variability in shallow water corals: Temperature dependence and growth-related vital effects. *Geochim. Cosmochim. Acta* **99**, 224–242 (2012).
99. A. N. Pettitt, A non-parametric approach to the change-point problem. *J. Royal Statist. Soc. Ser. C (Appl. Stat.)* **28**, 126–135 (1979).